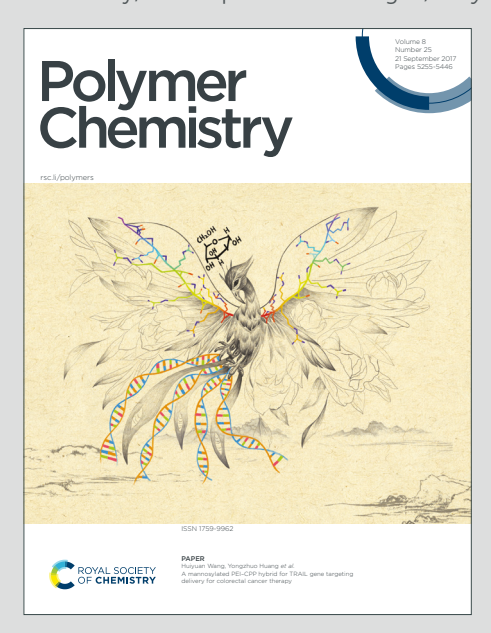


Polymer Chemistry



Accepted Manuscript

This article can be cited before page numbers have been issued, to do this please use: X. Wang, H. G. Abernathy, L. Kemp and S. E. Morgan, *Polym. Chem.*, 2024, DOI: 10.1039/D4PY00368C.



This is an Accepted Manuscript, which has been through the Royal Society of Chemistry peer review process and has been accepted for publication.

Accepted Manuscripts are published online shortly after acceptance, before technical editing, formatting and proof reading. Using this free service, authors can make their results available to the community, in citable form, before we publish the edited article. We will replace this Accepted Manuscript with the edited and formatted Advance Article as soon as it is available.

You can find more information about Accepted Manuscripts in the <u>Information for Authors</u>.

Please note that technical editing may introduce minor changes to the text and/or graphics, which may alter content. The journal's standard <u>Terms & Conditions</u> and the <u>Ethical guidelines</u> still apply. In no event shall the Royal Society of Chemistry be held responsible for any errors or omissions in this Accepted Manuscript or any consequences arising from the use of any information it contains.



View Article Online DOI: 10.1039/D4PY00368C

ARTICLE

Sprayable Adhesive Glycopolymer Hydrogels with Rapid In-Situ Gelation

Received 00th January 20xx, Accepted 00th January 20xx

DOI: 10.1039/x0xx00000x

Xianjun Wang, Hannah G. Abernathy, Lisa K. Kemp and Sarah E. Morgan*

Designing a sprayable, shear-thinning hydrogel with rapid in-situ gelation opens new opportunities for biomedical applications. Most traditional sprayable hydrogels require time-of-application mixing of reactive solutions, and they face inevitable material loss during application due to their slow gelation kinetics. In this study, we introduce a novel physically crosslinked hydrogel containing saccharide pendant groups characterized by a significant degree of shear-thinning behavior and fast modulus recovery under substantial shear deformation. This hydrogel can be sprayed easily via a commercially available atomizer, and the sprayed gel adheres to a vertically aligned polystyrene petri dish without dripping or flowing. The incorporation of sugar moieties not only contributes to maintaining the integrity of the gel network, but also facilitates dye penetration and enhances adhesive properties. By evaluating these interdependencies, this research demonstrates the intricate connections between polymer structural features, hydrogel properties, and processing as a sprayable material.

Introduction

Published on 29 May 2024. Downloaded by University of Southern Mississippi on 5/29/2024 5:42:33 PM

Polymeric hydrogels have tremendous promise for biomedical applications due to their remarkable capacity to imbibe large amounts of water and control drug release based on their unique physicochemical properties. The ability to use a spray application technique with hydrogels maximizes their potential as novel drug carriers by offering the flexibility to coat large and irregular areas for non-invasive drug delivery. Emerging applications for such systems include wound management, ¹⁻³ surgical hemostatic coatings, ⁴ and localized cell immobilization. ^{5, 6} Yet, striking a delicate balance between sprayability, gelation kinetics, and other crucial properties—such as surface adhesiveness, mechanical strength, and the desired release profile — poses a formidable challenge.

Among those properties, the gelation kinetics is the most crucial, because slow crosslinking can result in rapid material dispersion and impede localized application. The conventional approach to control gelation involves a two-step process: first spraying precursor solutions and then applying an external trigger (i.e., thermo-, photo-, or ionic crosslinking) to induce the sol-gel transition.⁷ Thermosensitive block copolymers, such as poly(ethylene oxide)—poly(propylene oxide)—poly(ethylene oxide) (i.e., Pluronic F-127), can be sprayed in the liquid form at 20 °C and undergo in-situ gelation around body temperature.⁸ However, this temperature dependent phase-transition typically takes 2-3 minutes to occur, yielding a physical gel with insufficient mechanical strength that drips before gelation.⁹⁻¹¹

A UV-triggered design starts with a sprayable formulation of precursor solution containing polymer with vinyl residues and a photo initiator, and the sol-gel transition occurs on the target surface by exposure to UV light.^{5, 12, 13} In this process gelation kinetics depend on the UV source and exposure conditions, making it less practical for large-scale applications. Another strategy is to form a double network hydrogel, where two polymer solutions are supplied from different nozzles to prevent early reaction and nozzle jamming.1, 2, 7 Crosslinking (i.e., electrostatic interaction, borax-diol chemistry, etc.) occurs at the interface of the two solutions, but this method typically has a long gelation time, ranging from 10-150 s to form a hydrogel thin film.^{1,4,7} Both strategies are suitable only for flat, stationary surfaces, and material flow can be problematic given the long gelation times needed. So far, it remains a great challenge to design systems capable of instant and in-situ gelation after spraying.

Shear-thinning hydrogels with instant self-healing ability have also been explored, where the hydrogel undergoes disassembly (decreases in viscosity) upon application of shear and then reassembles instantaneously (self-healing, regains a gel form) once shear forces are removed.14 disassembly-reassembly properties from varied come reversible crosslinking mechanisms, such as hydrogen bonds, 15 guest-host interactions, 16 hydrophobicity, 17 electrostatic interactions, 18 metal-ligand coordination, 19 as well as dynamic covalent chemistry (e.g., Schiff base, oxime linkage, and disulfide bonds). 20-23 This unique character enables applications such as bio-inks for 3D bio-printing or injectable drug delivery.^{24,} ²⁵ The typical shear rates for extrusion and clinically relevant injection are up to 10^3 s⁻¹ and 10^4 - 10^5 s⁻¹, respectively, while the shear rates for industrial spraying processes are 10⁴ -10⁶ s⁻¹. ^{26, 27} Theoretically, it is possible to fabricate a sprayable hydrogel with shear-thinning properties. Kim et al. reported an enzyme-

School of Polymer Science and Engineering, University of Southern Mississippi, Hattiesburg, MS, USA. E-mail: sarah.morgan@usm.edu.

Electronic Supplementary Information (ESI) available: [details of any supplementary information available should be included here]. See DOI: 10.1039/x0xx00000x

ARTICLE Journal Name

catalyzed crosslinking hydrogel and tailored the system to be both injectable and sprayable with a medical syringe and commercial airbrush nozzle. Supramolecular gels, made by self-assembled peptides or small organogelators also have been reported for spray applications. Despite these advancements and rich design principles based on crosslinking mechanisms, there are limited reports of sprayable, shearthinning hydrogels and much to learn regarding the structure-property-processing relationships.

Glycopolymers, synthetic polymers with pendent sugar moieties, have garnered attention for their applications in diverse biomedical fields.31 The stereochemistry and multivalent effect (i.e. glycocluster effect) of the saccharide motifs create unique molecular interactions with proteins, cell surfaces, and biological substrates.32-36 However, a dense grafting of sugars often leads to strong self-aggregation,³⁷ which potential drawback of causing unpredictable interactions with drugs loaded for delivery, but may also improve substrate adhesion and hydrogel formation. Glycoblock copolymers have been reported that show unique elastomeric properties, making them attractive for applications such as bulk tissue adhesives, sealants, and pressure sensitive bioadhesives.³⁸⁻⁴¹ Very recently, a low molecular weight statistical glycocopolymer has been engineered into a hydrogel for neural tissue repair application and injected into animal models. This work used glycan and nucleoside pendent groups with a small molecule crosslinker, and emphasized the role of H-bonding in supramolecular hydrogel formation.⁴²

Glycopolymers are attractive due to their excellent biocompatibility, hydrophilicity, and adhesive properties. Glycopolymer physical hydrogels with a high degree of shear thinning and rapid recovery may provide an innovative solution for spray applications. To our knowledge, such materials have not yet been reported, and there is need for increased understanding of the structure-property relationships for design of processable systems. In this study, novel glycopolymer hydrogels of different compositions were synthesized via free radical polymerization and evaluated in comparison to homopolymer analogues. Rheological properties, morphology, swelling behavior, dye loading and release properties, and adhesive performance are reported. Propotype spray properties are demonstrated, laying the foundation for design of new sprayable delivery systems.

Experimental

Materials

Published on 29 May 2024. Downloaded by University of Southern Mississippi on 5/29/2024 5:42:33 PM

N-(2-Hydroxyethyl)acrylamide (HEAA, 97%), potassium persulfate (KPS, >99.0%), N-isopropylacrylamide (NiPAm, > 99.0%), N,N,N',N'-tetramethylethylenediamine (TEMED, >99.5%), silver triflate (AgOTf, >98%) and acetobromo- α -d-galactose (AcGalBr, >93%) were purchased from Sigma-Aldrich. Methanol (CH3OH), sodium methoxide methanol solution (30 wt%), dichloromethane (DCM), tetrahydrofuran (THF) and molecular sieves (4Å, powder) were purchased from Thermo Scientific Chemicals. All chemicals were

used without further purification. The <code>acetyl-protected</code> glycomonomer, <code>2'-acrylamidoethyl-2,3,4/61tetp3-00-acetyl-36-00</code>

Glycohydrogel and Homopolymer Synthesis

Copolymer hydrogel networks of GalEAm with HEAA (pGal-co-HEAA) and GalEAm with NiPAm (pGal-co-NiPAm) and homopolymer analogues (pHEAA, pNiPAm, and pGal) were synthesized via free radical polymerization. Based on green chemistry principles, this polymerization is designed to take place in water at room temperature without inert gas purging prior to or during polymerization. Copolymerizations used a 1:1 monomer feed ratio, total monomer (1M), KPS (2 mol%), and TEMED (1 mol%) concentrations were held constants for all polymerizations. Monomer(s), KPS, and DI-water were added to a 4 mL closed vial and vortexed for 10 seconds. TEMED was added to the homogenized mixture using a micropipette, and then the mixture was left undisturbed at room temperature for 24 hours. Polymer structures are provided in Figure 1.

Figure 1 Structures of the synthesized polymers: pHEAA, pNiPAm, pGal, pGal-co-HEAA and pGal-co-NiPAm.

Sample Preparation

Polymers were purified by dialysis against DI-water for three days and then freeze-dried for structural and molecular weight characterization. The as-polymerized samples have a solid content of 18.6%, estimated from reaction contents. The aspolymerized samples were used directly for morphology characterization, swell testing, rheological characterization (frequency sweep), diffusion experiments, and tackiness evaluation without purification or dilution. The swollen samples were prepared by soaking as-polymerized hydrogel in 20 mL of DI-water for 5 days and decanting the liquid portion. The solid content of swollen hydrogels was determined based on the residual mass after heating to 120 °C via thermogravimetric analysis. Solid content analysis rather than gel fraction is generally preferred for physical gels.⁴⁴ Swollen samples were morphology characterization, characterization (frequency sweep and alternating strain test), and the spray test. Any additional sample preparation is specified in each experimental section.

Thermogravimetric Analysis (TGA)

Published on 29 May 2024. Downloaded by University of Southern Mississippi on 5/29/2024 5:42:33 PM

Journal Name ARTICLE

TGA profiles were obtained using a TA Instruments Discovery TGA 550 (New Castle, DE) under nitrogen using platinum HT pans. The changes in weight of the swollen hydrogel were monitored by heating from 25 to 140 °C with a temperature ramp of 10 °C min⁻¹. Solid content of the swollen hydrogel sample was determined by the residual mass ratio. Each sample was measured in triplicate.

NMR Spectroscopy

¹H NMR spectroscopy was performed on purified, freeze-dried polymers using a 600 MHz Bruker Advance III (TopSpin 3.1p17) spectrometer using (methyl sulfoxide)-d₆, deuterium oxide, or chloroform-d as solvents. Copolymer composition was determined by comparing integrations of the relative intensities of the saccharide acetyl proton (4.15 ppm) to that of the two protons on the acrylamide backbone (1.95 ppm). All NMR spectra were processed and analyzed using Mnova software.

Attenuated Total Reflectance Fourier Transform Infrared (ATR-FTIR) Spectroscopy

FTIR spectra of purified, freeze-dried polymers were obtained using a Thermo Scientific Nicolet iS50 FT-IR in ATR mode. Reported spectra are an average of 128 scans at a resolution of 1 cm⁻¹. FTIR data was then normalized and analyzed using Origin Lab 8.0.

Aqueous Size Exclusion Chromatography with Multiangle Laser Light Scattering (ASEC-MALLS)

Molecular weight of purified, freeze-dried glycopolymer was determined using ASEC-MALLS on an Agilent 1260 Infinity II LC system with a PL aquagel MIXED-OH column, a DAWN HELEOS-II light scattering detector (λ = 633 nm, Wyatt Technology Inc.), and an Optilab T-rEX refractometer (Wyatt Technology Inc.). TRIS buffer (pH = 8.0) with 0.01% (w/v) NaN₃ was used as the eluent at a flow rate of 0.5 mL min⁻¹, temperature of 20 °C, a sample concentration of 1 mg mL⁻¹, and an injection volume of 100 µL. The refractive index increment (dn/dc) value of pGal was determined by a Reichert ARIAS 500 refractometer to be 0.145 mL/g. Wyatt ASTRA SEC/LS software (version 7.1.4.8) was used to determine the number-average molecular weight (M_n), weight-average molecular weight (M_w), and polymer dispersity (D).

Static Light Scattering (SLS)

Measurements of light-scattering intensity were performed at 21 °C over the angular range 30–120° with a Brookhaven Bl-200SM research goniometer with Bl-APD avalanche photodiode detector equipped with a 35 mW He - Ne laser emitting vertically polarized light at wavelength $\lambda=633$ nm. pNiPAm was dissolved in THF at concentrations ranging from 0.1-0.6 mg/mL, filtered using a 0.22-micron filter and placed in a sealed glass test tube for the SLS experiment. The intensity measurements were calibrated against toluene. A Zimm plot was built to calculate the molecular weight of pNiPAm using a literature dn/dc value of 0.107 cm³/g. 45

Scanning Electron Microscopy (SEM)

View Article Online

Analysis of the copolymer hydrogel morphology was done using a Zeiss Sigma VP field-emission SEM with Thermo System 7 EDS and WDS X-ray detectors (Thermo-Fisher Scientific, Waltham, MA). Hydrogel samples Fig S1 A-B were as-polymerized samples and samples Fig S1 C-D were swollen samples. Each hydrogel sample was transferred into a 1.5 mL plastic sample tube and soaked in liquid N2 for 5 mins until completely frozen. The frozen hydrogel was lyophilized at a pressure of 91 mT for 24 hours using SP Scientific VirTis Benchtop Pro Freeze Dryer. After lyophilization, the sample was soaked in liquid N₂ for 5 mins and fractured in liquid N2 with a pair of tweezers. The fractured samples were carefully adhered to conductive tape, making sure the fractured surface faced up in the SEM sample holder. The SEM samples were carbon-coated using a Cressington Carbon Coater (coating pressure < 0.01 mbar, with 10 exposures of 10 seconds each). The pore diameters were analyzed using ImageJ Analysis (ImageJ, National Institute of Health, MD).

Swelling Test

Hydrogel samples (post-polymerization without dialysis) were oven-dried at 120 °C for 48 hours. The samples were soaked in DI-water at room temperature and weighed at regular intervals over a 10-hour period. The swelling value (S) was calculated based on the following equation 1:

$$S(gH_2O/gpolymer) = (W - W_{dry})/W_{dry}$$
 (eq. 1)

where W_{dry} and W refer to the weight of dry and hydrated polymer samples, respectively.⁴⁶

Rheology Characterization

Viscoelastic properties were evaluated using a strain-controlled ARES rheometer equipped with 25 mm parallel steel plates with a 0.5 ± 0.05 mm gap height. All rheology tests were performed at 21 °C, below the lower critical solution temperature (LCST) of the NiPAm homopolymer. The small amplitude oscillatory shear (SAOS) tests were carried out with a frequency sweep range of 1-100 rad/s with 10% strain (within the linear viscoelastic region (LVR)) with as-polymerized (post- polymerization without purification or dilution) and swollen hydrogels (soaked in DIwater for five days). The time sweep tests were recorded at two strain levels, 10% and 700%, at 1 Hz. The swollen hydrogel sample was first loaded with 10% strain for 100 seconds and immediately increased to 700% loading for 100 seconds. This

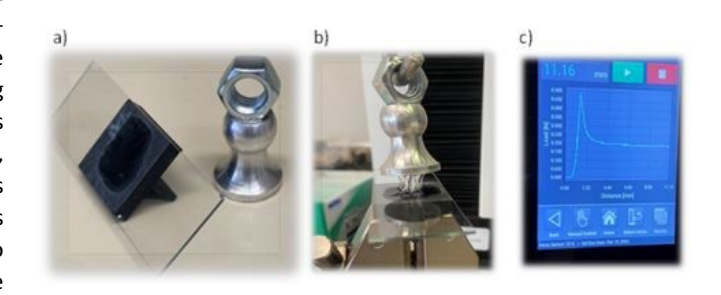


Figure 2 a) Tailored device for the pull off test. b) Test demonstration. c) A typical force-displacement trace recorded by the tensile tester.

ARTICLE Journal Name

cycle was repeated three times to evaluate hydrogel modulus recovery.

Tack Test

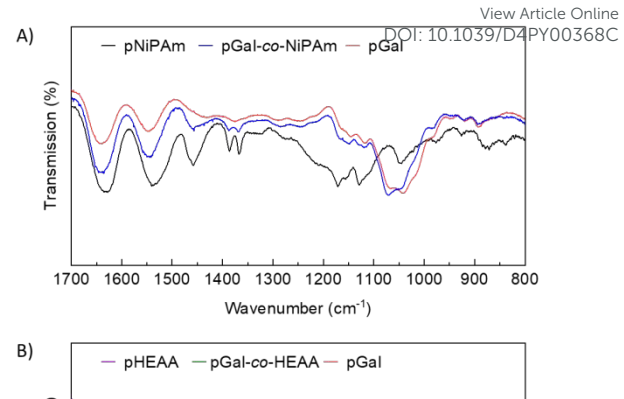
Tack testing was performed based on ASTM F2258 and D4541 using a Mark-10 EasyMESUR Test (Model F105) equipped with a 25 N load cell. Each hydrogel sample had a volume of 0.3 mL and was used after polymerization without purification or

m is initial loaded dye amount, v_0 is total volume of release media, v_e is the volume of release media removed at each time period, C_i(t) is the concentration of dye in the release media at time t, and C_n is the final concentration of dye in the release media.

Results and Discussion

Structural Characterization

FTIR data was used to qualitatively compare the structural components of each polymer type and determine the



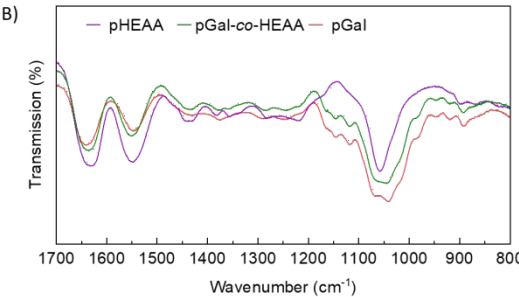


Figure 3 ATR-FTIR spectra of A) pNiPAm, pGal-co-NiPAm and pGal overlay plot. B) pHEAA, pGal-co-HEAA and pGal overlay plot. The two copolymers show a mixture of the features of the corresponding homopolymers, indicating successful

incorporation of monomers in the copolymers. In Figures 3 A and B, characteristic amide peaks are observed in all of the polymers, with the carbonyl stretching vibration present near 1630 cm⁻¹ and the N-H bending at approximately 1540 cm⁻¹. Neat pNiPAm shows characteristic peaks at 1458 (C-H from CH₂ or CH₃)⁴⁸ and 1367/1387 cm⁻¹ (CH(CH₃)₂) which correspond to asymmetric bending vibrations of isopropyl groups. 49 Glycohomopolymer shows a characteristic absorption pattern from 1200-800 cm⁻¹, symmetrical stretching of the ether linkage (i.e. C-O-C) at 1068 cm⁻¹, and alcohol linkage at 1018 cm⁻¹.⁵⁰ Neat pHEAA has a very strong CH2-OH stretching peak at 1058 cm-1, and the small peaks at 1468 and 1440 cm⁻¹ correspond to weak C-H stretching.⁵¹ Both copolymers show a mixture of the features of the corresponding homopolymers, suggesting

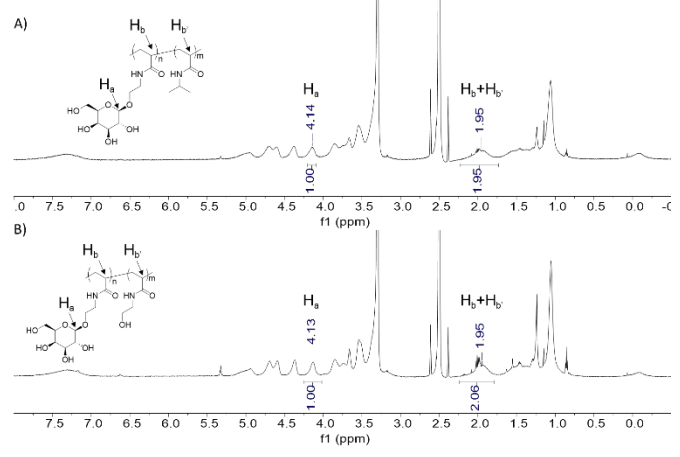


Figure 4 A) ¹H NMR spectrum of pGal-co-NiPAm; B) ¹H NMR spectrum of pGal-co-HEAA. Both polymers show the target comonomer incorporation.

Journal Name ARTICLE

High resolution solution state ¹H NMR spectroscopy was performed to determine monomer incorporation ratios within each copolymer. Purified and freeze-dried pGal-co-NiPAm completely dissolved in DMSO-d₆. However, pGal-co-HEAA was swollen in DMSO-d₆ with only a small amount of soluble fraction, which was used for NMR analysis and assumed to be representative of the copolymer composition. In Figures 4 A and B, the broad peak at 7.30 ppm is from the amide linkage (NH). The acetyl proton (H_a) from the saccharide unit is at 4.13/4.14 ppm and the four OH groups from the galactopyranoside can be clearly observed (4.36-4.96 ppm). Other protons at the galactopyranoside ring and the linkage (OCH₂CH₂, 3.84-3.20 ppm) cannot be clearly integrated due to overlap with the residual H₂O peak. The methine proton in the backbone (H_b and $H_{b'}$) shows a broad peak at 1.95 ppm, which is used to represent all repeat units. By comparing the integral of H_a and the backbone proton $(H_b + H_{b'})$, a 1:1 comonomer ratio is found for the soluble fractions of both copolymers.

A model polymerization of NiPAm under dilute conditions ([NiPAm] $_0$ = 0.5 M) was performed to qualitatively determine reaction time, and all vinyl groups were consumed after 30 minutes according to NMR analysis. For the hydrogel polymerizations (solid content of 18.6% w/v in water), the viscosity of the reaction mixture changed dramatically after the first 30 minutes of the polymerization and a similar reaction conversion of vinyl monomer was assumed.

Swelling Study

Published on 29 May 2024. Downloaded by University of Southern Mississippi on 5/29/2024 5:42:33 PM

Swelling tests were conducted with each of the synthesized polymers to evaluate their properties as physical hydrogels. The homopolymer data is not included because pNiPAm dissolved fully, the pHEAA became a very brittle thin film once exposed to water, and the pGal swelled very quickly (within one hour) but showed a decrease in mass with time suggesting that it was slowly dissolving. This indicates that the homopolymers do not form reversible hydrogels. The two copolymers, on the other hand, show equilibrium swelling behavior, shown in Fig 5. pGal-co-NiPAm displays increased water uptake and faster swelling behavior than pGal-co-HEAA. Polymers with pendant carbohydrate groups are reported to have an increased equilibrium swelling degree, attributed to their multiple hydroxyl groups.⁵² These results suggest that the structural features of GalEAm are crucial for maintaining the mechanical integrity of the copolymer physical gels. Furthermore, the

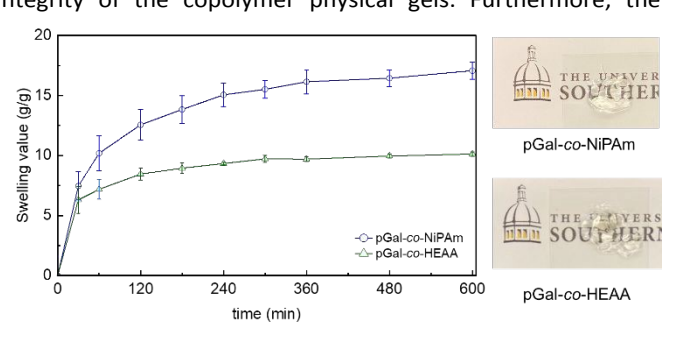


Figure 5 Kinetic water swelling test of pGal-co-NiPAm (blue circles) and pGal-co-HEAA (green triangles), n=3. pGal-co-NiPAm shows faster rehydration than pGal-co-HEAA after 60 min.

swelling kinetics of the gels can be adjusted by using Adifferent comonomers.

DOI: 10.1039/D4PY00368C

Rheological Characterization

A power law model is used to describe the relationship between storage modulus (G') and frequency (ω), shown in equation 3:

$$G' = A'\omega^{n'}$$
 (eq. 3)

where n' is the slope and logA' is the intercept in the log-log plot.

The as-polymerized copolymers (solid content of 18.6% w/v in water) exhibit similar rheological behavior, shown in Figure 6 A and B. The storage modulus remains higher than the loss modulus across the entire frequency range, without a crossover, indicating solid-like behavior and lack of a sol-gel transition. Both systems display a moderate dependence of modulus on frequency, where G' $\sim \omega^{0.224}$ for pGal-co-NiPAm and $G' \sim \omega^{0.239}$ for pGal-co-HEAA. These observed viscoelastic characteristics are consistent with a concentrated physically crosslinked system. 53, 54 The loss factor (tan δ) ranges from 0.23 to 0.37 over the probed frequency range for both copolymers, which is considered larger than that of a near-perfect network.55 After soaking both copolymers in an excess amount of DI-water for 5 days, the two swollen copolymers had 5.0% solid content and exhibited a decrease in storage modulus by an order of magnitude, shown in Figure 6 C and D, and maintained storage modulus higher than loss modulus across the entire frequency range. This behavior agrees with affine network theory, where the storage modulus scales with polymer volume fraction,^{56,57} and the addition of water reduces G' by decreasing the crosslink density through network swelling. The two copolymers show a clear plateau modulus after

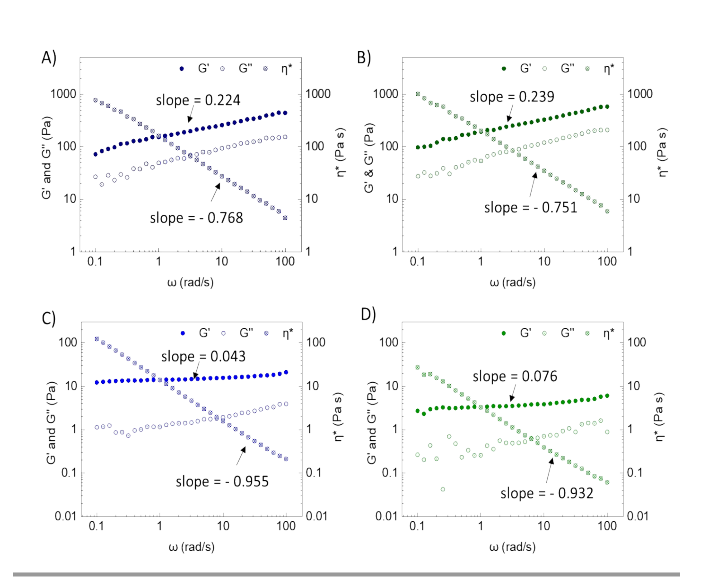


Figure 6 Frequency sweep of A) pGal-co-NiPAm after polymerization; B) pGal-co-HEAA after polymerization; The solid content of A) and B) is 18.6% based on reaction formulation. C) pGal-co-NiPAm after soaking in DI-water; D) pGal-co-HEAA after soaking in DI-water. The solid content of C) and D) are 5.0 \pm 0.10% and 5.0 \pm 0.05%, respectively, based on TGA measurement (n = 3). The two copolymers show G' – frequency independent character and a large degree of shear thinning after soaking in water.

ARTICLE Journal Name

swelling, with G' $^\sim \omega^{0.043}$ for pGal-co-NiPAm and G' $^\sim \omega^{0.076}$ for pGal-co-HEAA indicating very soft gels. 58

The zero-shear modulus was calculated by extrapolating the storage modulus to 0 rad/s, and the mesh size of the two highly swollen networks is estimated based on the correlation length using the elastic blob theory (Table 1). $^{59, 60}$ pGal-co-NiPAm is considered a stronger gel because of its slightly higher modulus, smaller tan δ , and smaller mesh size than those of the pGal-co-HEAA hydrogel. Statistical copolymers containing NiPAm and pendant saccharide moieties have been reported to form nanoscale aggregates at room temperature. 61 The pGal-co-NiPAm hydrogel may exhibit similar aggregation behavior due to incorporation of the more hydrophobic NiPAm, and those aggregates could serve as additional crosslinking sites in the hydrogel.

The complex viscosity decreases dramatically for both samples as ω increases. The Cox-Merz rule was applied, and the shear thinning index was calculated based on equation 4:

$$\eta = K \dot{\gamma}^{n-1} \tag{eq. 4}$$

where K is the consistency index, and n is the shear thinning index.

Increased shear-thinning is observed in the swollen hydrogels than in the as-polymerized samples (i.e., a more negative slope in the (η^*) vs (ω) log-log plot, Fig 6 C and D). In addition to reducing the crosslinking density by swelling, the additional water molecules may also interrupt intermolecular associations, resulting in smaller n values for both copolymers. Shear thinning index of as-polymerized copolymer gels are reported in Table S1.

 $\label{thm:constraints} \textbf{Table 1} \ \textbf{Rheological parameters of the swollen copolymer gels}$

Published on 29 May 2024. Downloaded by University of Southern Mississippi on 5/29/2024 5:42:33 PM

	Zero shear modulus (G ₀ ', Pa)	Mesh size (nm)	Shear thinning index (n)
pGal- <i>co</i> -NiPAm	1.148	152	0.043
pGal- <i>co</i> -HEAA	0.565	192	0.068

Alternating Strain Sweep Test and Spray Test

As shear levels vary over several orders of magnitude during the spraying process, it is important to understand hydrogel response and recovery in the presence and removal of applied strain. We employed a multicycle alternating step strain experiment at two levels of strain, 10% (non-destructive, within LVR) and 700% (destructive, large shear deformation), and evaluated modulus as a function of time. Both glycohydrogels retain solid-like character at both strain levels (G'>G"), showing an initial drop in G' at 700% strain followed by recovery, and complete G' recovery immediately upon reduction to 10% strain (Fig 7 A and B). At 700% strain, both copolymers show increased G" as well as decreased G', indicating that at higher strain levels (such as at the spray nozzle), a cross-over could occur, and the material would become more liquid-like. Time dependent behavior is more obvious for pGal-co-NiPAm, as it shows a larger change in G' when a large deformation is applied. The alternating step strain test reveals the intrinsic self-healing

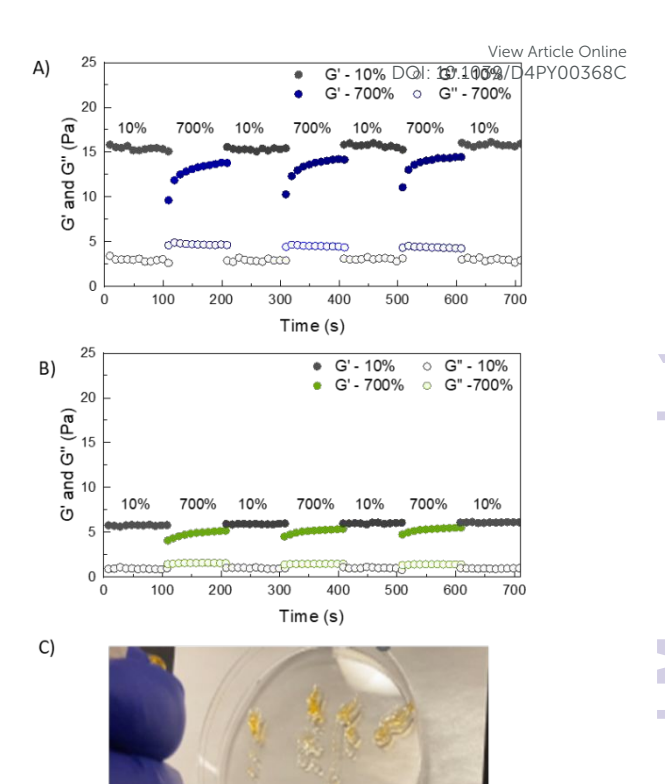


Figure 7 Alternating step strain of A) pGal-co-NiPAm, and B) pGal-co-HEAA. The two copolymers show multicycle moduli recovery under a large degree of shear deformation. C) "Jet-like" spray pattern of pGal-co-NiPAm.

nature of these two glycohydrogels, which is consistent with the reversible physical crosslinking design.⁶²⁻⁶⁴

The rheological results also indicate that these materials could be highly suitable for spray applications. A 2 mL commercially available spray bottle atomizer was used to spray pGal-co-NiPAm onto a vertically aligned polystyrene petri dish. To enhance visibility, a drop of methyl orange dye was added to the highly transparent hydrogel before spraying. Figure 7 C shows the spray pattern, and the full video of the test is provided in the supplemental information (Video S1). The geometry of the nozzle, pressure drop, flow rate, and rheological characteristics of the dispensed material are known to affect the spraying pattern.65 The pGal-co-NiPAm hydrogel exhibits little to no flow after the sprayed droplets contact the polystyrene surface, suggesting that after passing through the fine atomizer, the hydrogel rapidly returns to its gelled state. We also sprayed pGal-co-NiPAm hydrogel onto a pothos leaf, a biological surface with moderate hydrophobicity, and pGal-co-NiPAm showed no dripping after application (Figure S3).

Visualization of Hydrogel Morphology

SEM is used to visualize the morphological features of the hydrogel samples, and the pore diameters were defined as the smallest diameter of the void space enclosed.⁶⁶ After polymerization, pGal-co-NiPAm shows irregular porous features with more sub-voids below the fracture surface, and pGal-co-

Journal Name ARTICLE

HEAA shows circular pore shapes with thicker walls, shown in Fig. S1. The pore diameters of pGal-co-NiPAm and pGal-co-HEAA are 0.81 \pm 0.15 μm and 1.25 \pm 0.44 μm , respectively, but the difference in the means is not statistically significant. After swelling, both copolymers maintain porous features. pGal-co-NiPAm shows two types of voids: large, distorted hexagonal features and smaller voids within the hexagon walls. pGal-co-HEAA shows irregular and interconnected hollow features.

The hydrogel mesh size was determined from a bulk rheology experiment based on elastic blob theory, which represents the elastically effective chain length of a network. Mesh size should not be confused with the porous features directly observed from SEM. Pores are larger voids in the structure with a diameter on the μm scale and the pore wall consists of bundles of aggregated polymers.⁶⁰ In our case, the pores observed by SEM are due to ice-templating, where the aggregated polymers are pushed together by ice crystal formation during SEM sample preparation and are not necessarily representative of the structure of the hydrogel when hydrated. However, the mesh size is concerned with individual chains and typically on a nm scale, closer to the size of species exchanged through a hydrogel network, such as dyes, drugs, or other bioactive species when the hydrogel is in a hydrated state.^{59,67} Therefore, mesh size can significantly affect the loading capacity and the release kinetics of the solute.

Understanding Gel Formation

Published on 29 May 2024. Downloaded by University of Southern Mississippi on 5/29/2024 5:42:33 PM

Distinct differences among the three homopolymers were observed; pGal slowly dissolves in DI-water over a 5-day period, pNiPAm does not form a hydrogel, and pHEAA is a very brittle thin film after attempted rehydration. These differences in gel formation are attributed to the hydrogen bonding preferences (intermolecular and intramolecular) exhibited by these high molecular weight polymers. Intrachain hydrogen bonding in pHEAA has been reported to reduce water solubility.⁶⁸ Our team previously reported the extensive aggregation and gelation behavior of pGal, driven by intramolecular H-bonding of the pendant saccharide moieties and hydrophobic effects of the polymer backbone.⁶⁹

ASEC-MALLS was attempted for the three homopolymers in buffer solution, but due to solubility issues of the pNiPAm and the pHEAA, it was possible to obtain molecular weight measurements only for pGal, which displayed $M_{\rm n}$ of 1.71 x10 6 g/mol, $M_{\rm w}$ of 3.40 x 10 6 g/mol, and θ of 1.99 (Figure S2). The absolute molecular weight of pNiPAm was determined using SLS and found to be 2.11 x 10 6 g/mol, similar to that of pGal. It was not possible to solubilize pHEAA in buffer solution and common organic solvents, and we were unable to find a common solvent for the copolymers. Given that all samples were created using the same polymerization conditions, it is reasonable to assume that all polymers have high molecular weights similar to that of the pGal and pNiPam.

There does not appear to be any evidence of compositional draft in the copolymerization that might affect solubility. Unlike pNiPAm homopolymers or blocky polymers containing pNiPAm segments, no phase change was observed for the swollen pGalco-pNiPAm hydrogel with changing temperatures (i.e. 5-50 °C).,

and literature reports indicate polymerization of comonomers (including glycomonomers⁷⁰) with similar acryla คำใช้ยารัสธ์เหอร์ครร tend to yield statistical monomer unit distributions.⁶¹

Therefore, we attribute the gel formation of the two copolymers to chain entanglement in the high molecular weight systems, H-bonding interactions, and the hydrophobic effect. Introducing HEAA into the copolymer should lead to more polymer-polymer H-bonding interactions, making the copolymers less soluble in water, while introducing NiPAm into the copolymer is expected to increase the hydrophobic effect, making pGal-co-NiPAm a slightly stronger gel.

Dye Loading and Release

A pair of ionic water-soluble dyes, methyl orange (with an anionic core) and methylene blue (with a cationic core), were selected to investigate loading and release behavior of the aspolymerized hydrogels. For the pHEAA and pNiPAm homopolymers, methylene blue precipitated from solution and methyl orange showed only limited uptake, so these systems were not included in the dye studies. In contrast, both dyes were successfully absorbed in pGal and the two copolymer hydrogels under the same incubation conditions, indicating that the galactose group aids in dye diffusion into the viscoelastic matrix. A similar phenomenon was reported by Cook et al., where incorporating 20% N-acryloyl-D-glucosamine in a chemically crosslinked hydrogel promoted uniform dispersion of fluorescein isothiocyanate-dextran in the matrix, resulting in a more uniform fluorescence signal compared to the control. The carbohydrate-aromatic interaction may explain why dyes show better distribution in pGal, pGal-co-HEAA and pGal-co-NiPAm. This non-covalent interaction between C-H groups from pyranoses and π electrons of the electron-rich aromatic ring plays a pivotal role in bimolecular recognition between carbohydrates and peptides or proteins.71, 72 Hudson et al investigated the interaction between β-D-galactose with amino acids and found β -D-galactose would interact preferentially with electron rich aromatic residues (i.e. tryptophan).73 Bromfield et al reported both carbohydrate-aromatic interactions and charge-charge electrostatic interactions contributed to effective binding between Mallard Blue dye and heparin (a glycosaminoglycan).74 For pHEAA and pNiPAm homopolymers, which contain no glycomonomer, precipitation of the dye occurred. Based on diffusion theory, water should diffuse much faster than dye due to a much lower molecular weight; therefore, it is likely the dye reservoir became more and more concentrated until the dye precipitated from the matrix.

Results of the cumulative release study of pGal and copolymers are shown in Figure 8 A and B. pGal shows faster release with both dyes, followed by pGal-co-HEAA and pGal-co-NiPAm. This observation is consistent with the swelling tests and rheological experiments. pGal quickly rehydrates, followed by slow dissolution; therefore, the dye release from pGal is accompanied by a matrix dissolution, resulting in the fastest release kinetics. The two copolymers form stable networks with varied mesh sizes, and do not dissolve during the diffusion experiment. pGal-co-NiPAm has smaller mesh size, resulting in a slower releasing pattern than that of pGal-co-HEAA. Another

View Article Online DOI: 10.1039/D4PY00368C

ARTICLE Journal Name

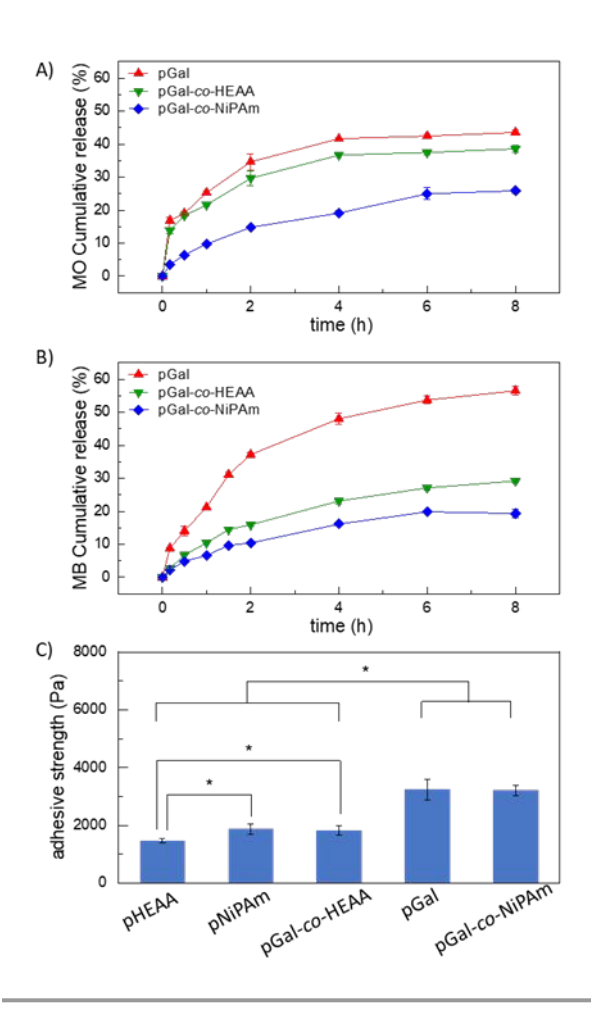


Figure 8 A) Cumulative release of methyl orange; B) Cumulative release of methylene blue. C) Adhesive strengths of five hydrogels, n = 5. Asterisks above bars represent statistically significant data (p < 0.05).

potential contributing factor is that the saccharide pendant group in pGal has weaker interactions with the dyes than those of the CH₂CH₂OH or CH(CH₃)₂ pendant groups of pHEAA and pNiPAm. These results indicate that incorporating a saccharide pendant unit in the polymer may be advantageous for drug delivery applications.

Evaluation of Hydrogel Tackiness

Published on 29 May 2024. Downloaded by University of Southern Mississippi on 5/29/2024 5:42:33 PM

After polymerization, each of the hydrogels exhibited a high degree of tackiness. To measure the adhesive strength of the hydrogels, a modified tensile test was conducted. The adhesive strength was determined by dividing the maximum pull-off force by the contact area to determine the resistance when separating two glass substrates with a fixed hydrogel contact area. The relative adhesive strength of the three homopolymers is: pGal > pNiPAm > pHEAA, shown in Figure 8C. pGal-co-NiPAm shows adhesive strength similar to that of pGal homopolymer, but pGal-co-HEAA shows reduced adhesive strength, in the range of that of pNiPAm homopolymer. These findings indicate that the saccharide pendant groups allow effective binding to the glass substrate through their multiple hydrogen bonding moieties, and that the strength of the binding can be adjusted with copolymer composition.

Conclusions

A novel shear responsive design was devised to overcome current challenges of sprayable hydrogels. Green chemistry principles were applied in this research, where biocompatible building blocks were selected and polymerizations were performed under ambient conditions (aqueous, room temperature, no N₂ purging). Reversible physical gels were obtained only for the glyco-copolymers, which we attribute to chain entanglements due to high molecular weight, hydrogen bonding, and hydrophobic effects. Gel strength, mesh size, swelling rate, and morphology were found to be a function of copolymer composition. Rheological studies of the swollen hydrogels revealed a significant degree of shear thinning and instantaneous self-healing in step-strain evaluations, properties which are highly desirable for spray applications. A proof-ofconcept spray test demonstrated that the pGal-co-NiPAm copolymer was readily sprayed onto an inclined hydrophobic surface (i.e. the PS surface and a pothos leaf) without apparent dripping, and adhesive testing demonstrated improved adhesive strength of the copolymer gels in comparison to homopolymer analogues. Tunable dye uptake and release kinetics, facilitated by the carbohydrate-aromatic interaction, was dependent on glycopolymer structure, indicating the potential for tailored delivery. The combined results demonstrate the strong potential for glyco-copolymer hydrogels in the design of sprayable hydrogels for delivery applications.

Conflicts of interest

There are no conflicts to declare.

Acknowledgements

We gratefully acknowledge financial support from the National Institutes of Health Grant No. 1R15Al167013-01A1. This work was also supported by the Mississippi INBRE, funded by an Institutional Development Award (IDeA) from the National Institute of General Medical Sciences of the National Institutes of Health under grant number P20GM103476.

References

- 1. C. Cai, T. Wang, X. Han, S. Yang, C. Lai, T. Yuan, Z. Feng and N. He, *Chin. Chem. Lett.*, 2022, **33**, 1963-1969.
- Z. Liu, W. Tang, J. Liu, Y. Han, Q. Yan, Y. Dong, X. Liu, D. Yang, G. Ma and H. Cao, *Bioact. Mater.*, 2023, 20, 610-626.
- 3. J. J. He, C. McCarthy and G. Camci-Unal, *Adv. Nano Res.*, 2021, **1**, 2100004.
- G. Muñoz Taboada, P. Dosta, E. R. Edelman and N. Artzi, Adv. Mater., 2022, 34, 2203087.
- M. O. Pehlivaner Kara and A. K. Ekenseair, J. Biomed. Mater. Res. A, 2016, 104, 2383-2393.
- 6. S. Ishikawa, H. Kamata, U.-i. Chung and T. Sakai, *ACS Appl. Bio Mater.*, 2023, **6**, 4613-4619.
- 7. H. Geng, Q. Dai, H. Sun, L. Zhuang, A. Song, F. Caruso, J. Hao and J. Cui, *ACS Appl. Bio Mater.*, 2020, **3**, 1258-1266.

Published on 29 May 2024. Downloaded by University of Southern Mississippi on 5/29/2024 5:42:33 PM

Journal Name

- 8. Y. L. Wong, M. Pandey, H. Choudhury, W. M. Lim, S. K. Bhattamisra and B. Gorain, *Polymers (Basel)*, 2021, **13**, 2770.
- 9. T. Murakami, T. Kawamori, J. D. Gopez, A. J. McGrath, D. Klinger and K. Saito, *J. Polym. Sci., Part A: Polym. Chem.*, 2018, **56**, 1033-1038.
- 10. A. Colly, C. Marquette and E.-J. Courtial, *Langmuir*, 2021, **37**, 4154-4162.
- 11. A.-L. Kjøniksen, M. T. Calejo, K. Zhu, B. Nyström and S. A. Sande, *J. Appl. Polym. Sci.*, 2014, **131**, 40465.
- 12. H. Cheng, Z. Shi, K. Yue, X. Huang, Y. Xu, C. Gao, Z. Yao, Y. S. Zhang and J. Wang, *Acta Biomater.*, 2021, **124**, 219-232.
- 13. N. Annabi, D. Rana, E. Shirzaei Sani, R. Portillo-Lara, J. L. Gifford, M. M. Fares, S. M. Mithieux and A. S. Weiss, *Biomaterials*, 2017, **139**, 229-243.
- 14. C. Loebel, C. B. Rodell, M. H. Chen and J. A. Burdick, *Nat. Protoc.*, 2017, **12**, 1521-1541.
- 15. D. Wang, Y. Xia, D. Zhang, X. Sun, X. Chen, S. Oliver, S. Shi and L. Lei, *ACS Appl. Polym. Mater.*, 2020, **2**, 1587-1596.
- 16. X. Jiang, F. Zeng, X. Yang, C. Jian, L. Zhang, A. Yu and A. Lu, *Acta Biomater.*, 2022, **141**, 102-113.
- 17. A. K. Mahanta and P. Maiti, *ACS Appl. Bio Mater.*, 2019, **2**, 5415-5426
- 18. Y. Zhu, Q. Luo, H. Zhang, Q. Cai, X. Li, Z. Shen and W. Zhu, *Biomater. Sci.*, 2020, **8**, 1394-1404.
- 19. L. Shi, Y. Zeng, Y. Zhao, B. Yang, D. Ossipov, C.-W. Tai, J. Dai and C. Xu, *ACS Appl. Mater. Interfaces*, 2019, **11**, 46233-46240.
- 20. B. Fan, D. Torres García, M. Salehi, M. J. Webber, S. I. van Kasteren and R. Eelkema, *ACS Chem. Biol.*, 2023, **18**, 652-659.
- 21. S. Uman, A. Dhand and J. A. Burdick, *J. Appl. Polym. Sci.*, 2020, **137**, 48668.
- 22. C. Yang, L. Gao, X. Liu, T. Yang, G. Yin, J. Chen, H. Guo, B. Yu and
- H. Cong, J. Biomed. Mater. Res. A, 2019, **107**, 1909-1916. 23. G. N. Grover, R. L. Braden and K. L. Christman, Adv. Mater., 2013,
- **25**, 2937-2942.
- 24. M. H. Chen, L. L. Wang, J. J. Chung, Y.-H. Kim, P. Atluri and J. A. Burdick, *ACS Biomater. Sci. Eng.*, 2017, **3**, 3146-3160.
- 25. M. A. Habib and B. Khoda, *J. Manuf. Process.*, 2022, **76**, 708-718. 26. H. Lopez Hernandez, J. W. Souza and E. A. Appel, *Macromol. Biosci.*, 2021, **21**, 2000295.
- 27. V. Carnicer, C. Alcázar, M. J. Orts, E. Sánchez and R. Moreno, *Open Ceramics*, 2021, **5**, 100052.
- 28. S.-H. Kim, S.-H. Lee, J.-E. Lee, S. J. Park, K. Kim, I. S. Kim, Y.-S. Lee, N. S. Hwang and B.-G. Kim, *Biomaterials*, 2018, **178**, 401-412.
- 29. C. F. Anderson, R. W. Chakroun, M. E. Grimmett, C. J. Domalewski, F. Wang and H. Cui, *Nano Lett.*, 2022, **22**, 4182-4191.
- 30. H. Sun, J. Jiang, L. Zhang, C. Yuan, Y. Jiang and P. Liu, *Colloids Surf. A Physicochem. Eng. Asp.*, 2022, **640**, 128460.
- 31. I. Pramudya and H. Chung, Biomater. Sci., 2019, 7, 4848-4872.
- 32. M. H. Stenzel, Macromolecules, 2022, 55, 4867-4890.
- 33. L. L. Kiessling and J. C. Grim, *Chem. Soc. Rev.*, 2013, **42**, 4476-4491.
- 34. J. Becker, R. Terracciano, G. Yilmaz, R. Napier and C. R. Becer, *Biomacromolecules*, 2023, **24**, 1924-1933.
- 35. H. Lis and N. Sharon, Chem. Rev., 1998, 98, 637-674.
- 36. S. R. S. Ting, G. Chen and M. H. Stenzel, *Polym. Chem.*, 2010, 1, 1392-1412.
- 37. T. Oh, Y. Hoshino and Y. Miura, *J. Mater. Chem. B*, 2020, **8**, 10101-10107.
- 38. C. Deng, F. Li, J. M. Hackett, S. H. Chaudhry, F. N. Toll, B. Toye, W. Hodge and M. Griffith, *Acta Biomater.*, 2010, **6**, 187-194.
- 39. N. Pokeržnik and M. Krajnc, Eur. Polym. J., 2015, **68**, 558-572.
- 40. M. Nasiri and T. M. Reineke, *Polym. Chem.*, 2016, **7**, 5233-5240.

41. I. Pramudya, C. Kim and H. Chung, *Polym. Chem.*, 2018, 9, 3638-3650.

ARTICLE

- 42. E. M. DuBois, H. O. Adewumi, P. R. O'Connor, J. E. Labovitz and T. M. O'Shea, *Adv. Mater.*, 2023, **35**, 2211774.
- 43. P. K. Das, D. N. Dean, A. L. Fogel, F. Liu, B. A. Abel, C. L. McCormick, E. Kharlampieva, V. Rangachari and S. E. Morgan, *Biomacromolecules*, 2017, **18**, 3359-3366.
- 44. C. Wang, T. Hashimoto, Y.-C. Chuang, K. Tanaka, Y.-P. Chang, T.-W. Yang and M.-T. Huang, *Macromolecules*, 2022, **55**, 9152-9167.
- 45. K. Kubota, S. Fujishige and I. Ando, Polym. J., 1990, 22, 15-20.
- 46. A. Bal, B. Özkahraman and Z. Özbaş, J. Appl. Polym. Sci., 2016, 133.
- 47. H. Yuk, C. E. Varela, C. S. Nabzdyk, X. Mao, R. F. Padera, E. T. Roche and X. Zhao, *Nature*, 2019, **575**, 169-174.
- 48. M. M. Rana, A. Rajeev, G. Natale and H. De la Hoz Siegler, *J. Mater. Res. Technol.*, 2021, **13**, 769-786.
- 49. M. Liu, F. Bian and F. Sheng, *Eur. Polym. J.*, 2005, **41**, 283-291.
- 50. T. Hong, J.-Y. Yin, S.-P. Nie and M.-Y. Xie, *Food Chem.: X*, 2021, **12**, 100168.
- 51. C. Zhao, Q. Chen, K. Patel, L. Li, X. Li, Q. Wang, G. Zhang and J. Zheng, *Soft Matter*, 2012, **8**, 7848-7857.
- 52. M. T. Cook, S. L. Smith and V. V. Khutoryanskiy, *Chem. Comm.*, 2015, **51**, 14447-14450.
- 53. A. C. Yu, A. A. A. Smith and E. A. Appel, *Mol. Syst. Des. Eng.*, 2020, **5**, 401-407.
- 54. S. Derkach, I. Zhabyko, N. Voron'ko, A. Maklakova and T. Dyakina, *Colloids Surf. A: Physicochem. Eng.*, 2015, **483**, 216-223.
- 55. M. Rubinstein and R. H. Colby, *Polymer Physics*, Oxford University Press, 2003.
- 56. F. Tanaka, *Polymer Physics: Applications to Molecular Association and Thermoreversible Gelation*, Cambridge University Press, Cambridge, 2011.
- 57. G. Song, Z. Zhao, X. Peng, C. He, R. A. Weiss and H. Wang, *Macromolecules*, 2016, **49**, 8265-8273.
- 58. E. R. Morris, K. Nishinari and M. Rinaudo, *Food Hydrocoll.*, 2012, **28**, 373-411.
- 59. P. J. Moncure, Z. C. Simon, J. E. Millstone and J. E. Laaser, *J. Phys. Chem. B*, 2022, **126**, 4132-4142.
- 60. Y. Tsuji, X. Li and M. Shibayama, Gels, 2018, 4, 50.
- 61. M. Arcos-Hernandez, P. Naidjonoka, S. J. Butler, T. Nylander, H. Stålbrand and P. Jannasch, *Biomacromolecules*, 2021, **22**, 2338-2351.
- 62. P. Bertsch, M. Diba, D. J. Mooney and S. C. G. Leeuwenburgh, *Chem. Rev.*, 2023, **123**, 834-873.
- 63. Z. Jing, A. Xu, Y.-Q. Liang, Z. Zhang, C. Yu, P. Hong and Y. Li, *Polymers (Basel)*, 2019, **11**, 952.
- 64. S. Aihua, X. Dai and Z. Jing, *Polym. Sci. A*, 2020, **62**, 228-239.
- 65. R. Shai and N. Benveniste, presented in part at the 34th Joint Propulsion Conference, 1998.
- 66. I. Jayawardena, P. Turunen, B. C. Garms, A. Rowan, S. Corrie and L. Grøndahl, *Mater. Adv.*, 2023, **4**, 669-682.
- 67. J. Karvinen, T. O. Ihalainen, M. T. Calejo, I. Jönkkäri and M. Kellomäki, *Mater. Sci. Eng. C*, 2019, **94**, 1056-1066.
- 68. N. Saito, T. Sugawara and T. Matsuda, *Macromolecules*, 1996, **29**, 313-319.
- 69. A. N. Bristol, J. Saha, H. E. George, P. K. Das, L. K. Kemp, W. L. Jarrett, V. Rangachari and S. E. Morgan, *Biomacromolecules*, 2020, **21**, 4280-4293.
- 70. T. Newton, K. Green, A. Kulkarni, L. K. Kemp and S. E. Morgan, presented in part at the ACS Spring National Meeting, New Orleans, 2024.
- 71. J. L. Asensio, A. Ardá, F. J. Cañada and J. Jiménez-Barbero, *Acc. Chem. Res.*, 2013, **46**, 946-954.

Journal Name

View Article Online

DOI: 10.1039/D4PY00368C

ARTICLE

72. A. P. Davis, Chem. Soc. Rev., 2020, 49, 2531-2545.

D. K. Smith, JACS, 2013, 135, 2911-2914.

73. K. L. Hudson, G. J. Bartlett, R. C. Diehl, J. Agirre, T. Gallagher, L. L.

Kiessling and D. N. Woolfson, *JACS*, 2015, **137**, 15152-15160. 74. S. M. Bromfield, A. Barnard, P. Posocco, M. Fermeglia, S. Pricl and